

Periodic Barrier Structure in AA-Stacked Bilayer Graphene

Ilham Redouani^a and Ahmed Jellal^{*a,b}

^a*Theoretical Physics Group, Faculty of Sciences, Chouaib Doukkali University,
PO Box 20, 24000 El Jadida, Morocco*

^b*Saudi Center for Theoretical Physics, Dhahran, Saudi Arabia*

Abstract

We study the charge carriers transport in an AA-stacked bilayer graphene modulated by a lateral one-dimensional multibarrier structure. We investigate the band structures of our system, that is made up of two shifted Dirac cones, for finite and zero gap. We use the boundary conditions to explicitly determine the transmission probability of each individual cone ($\tau = \pm 1$) for single, double and finite periodic barrier structure. We find that the Klein tunneling is only possible when the band structure is gapless and can occur at normal incidence as a result of the Dirac nature of the quasiparticles. We observe that the band structure of the barriers can have more than one Dirac points for finite periodic barrier. The resonance peaks appear in the transmission probability, which correspond to the positions of new cones index like associated with $\tau = \pm 1$. Two conductance channels through different cones ($\tau = \pm 1$) are found where the total conductance has been studied and compared to the cases of single layer and AB-stacked bilayer graphene.

PACS numbers: 72.80.Vp, 71.10.Pm, 03.65.Pm

Keywords: AA-stacked bilayer graphene, multibarriers, transmission, Klein effect, conductance.

*ajellal@ictp.it – a.jellal@ucd.ac.ma

1 Introduction

Graphene, single layer of pure carbon atoms in a honeycomb lattice, has a gapless linear electronic spectrum near to the two valleys of the first Brillouin zone [1–3]. That yields electrons in graphene are described by a massless two dimensional relativistic Dirac equation and the corresponding electrons have a chiral nature [4,5]. This leads to many unusual electronic properties and potential applications [2,3]. Another interesting property is the Klein tunneling [6], describing that the Dirac fermions can be transmitted with probability one through a classically forbidden region. Graphene can not only exist in the free state, but two or more layers can stack above each other to form what is called few-layer graphene, as example bilayer graphene is resulting from a composition of two stacked sheets. Bilayer graphene has surged as another attractive two-dimensional carbon material. In addition, it is demonstrated that the bilayer graphene has a new unusual physical properties and the spectrum is different from that of single layer graphene. There are two dominant ways in which the two layers can be stacked: the AB-stacked and AA-stacked bilayer graphene.

AB-stacked bilayer graphene or Bernal form is the basis of the graphite from [7] and is usually derived. In which only one atom in the lower layer lies directly below an other atom in the upper layer and the other two atoms over the center of the hexagon in the other layer. AB-stacked bilayer graphene has a gapless quadratic dispersion relation, two conduction bands and two valance bands, each pair is separated by an interlayer coupling energy of order $\gamma_1 = 0.4 \text{ eV}$. Recent experiments showed that the AA-stacked bilayer graphene could also exist and is a new stable stacking of graphene [8–13], where the A sublattice of the top layer is stacked directly above the same sublattice of the bottom layer. In AA-stacked bilayer graphene, the energy bands are just the double copies of single layer graphene bands shifted up and down by the interlayer coupling $\gamma = 0.2 \text{ eV}$. Additionally, it has band structures that differ from those corresponding to single layer and AB-stacked bilayer graphene.

Recently, many works have been reported in order to investigate the multibarrier structures in single layer graphene [14–21]. However, much less experimental and theoretical works have been done on AB-stacked bilayer graphene [21,22]. Motivated by different developments on the subject and in particular [14,23,24], we investigate the energy bands for finite and zero gaps in AA-stacked bilayer graphene. Our theoretical model is based on the well established tight binding Hamiltonian [23–26] and we adopt the parametrization of the relevant intralayer and interlayer couplings. We note that the electronic band structure can be modified by the application of a periodic potential and the gaps. We explicitly calculate the transmission probability of each individual cone ($\tau = \pm 1$) for single, double and finite periodic barrier structure. We show that the Klein tunneling is only possible when the band structure is gapless and can occur at normal incidence. This makes difference with respect to the case of AB-stacked bilayer graphene where no Klein tunneling ($T = 1$) is expected [21,27]. We show that the existence of the intracone transition allows only two transmission channels in AA-stacked bilayer graphene resulting in a total conductance, while the transmission in the intercone is zero. In contrast, for AB-stacked bilayer graphene [27] we have intracone and intercone transitions, which are possible between all four bands. In addition, the total conductance of AA-stacked bilayer graphene is different with that of the single layer graphene [14].

The rest of the paper is organized as follows. In section 2, we consider the multibarrier structure for the AA-stacked bilayer graphene. We formulate our model by setting the Hamiltonian system

and calculating the associated energy bands in each potential region. We obtain the spinor solution corresponding to each regions. Using the transfer matrix at boundaries together with the incident, transmitted and reflected currents we end up with two transmission probabilities. In section 3, we numerically present our results of the transmission probability of each individual cone for single, double and finite periodic barrier structure. In section 4, based on the obtained results we study two conductance channels through different cones and as well as the corresponding total conductance. We conclude our work in the final section.

2 Energy bands

We consider electron tunneling through a lateral one-dimensional multibarrier in AA-stacked bilayer graphene as shown in Figure 1(c), consisting of $N + 2$ regions indexed by r . The parameters for the regions represented by an odd index $r = 2n_- + 1$, are the potential barrier heights V_{2n_-+1} , the widths d and the gaps Δ_{2n_-+1} . However, for an even index, we have $V_{2n_+} = \Delta_{2n_+} = 0$, where $n_{\pm} = \{0, 1, \dots, \frac{N+1}{2}\}$, with the widths a .

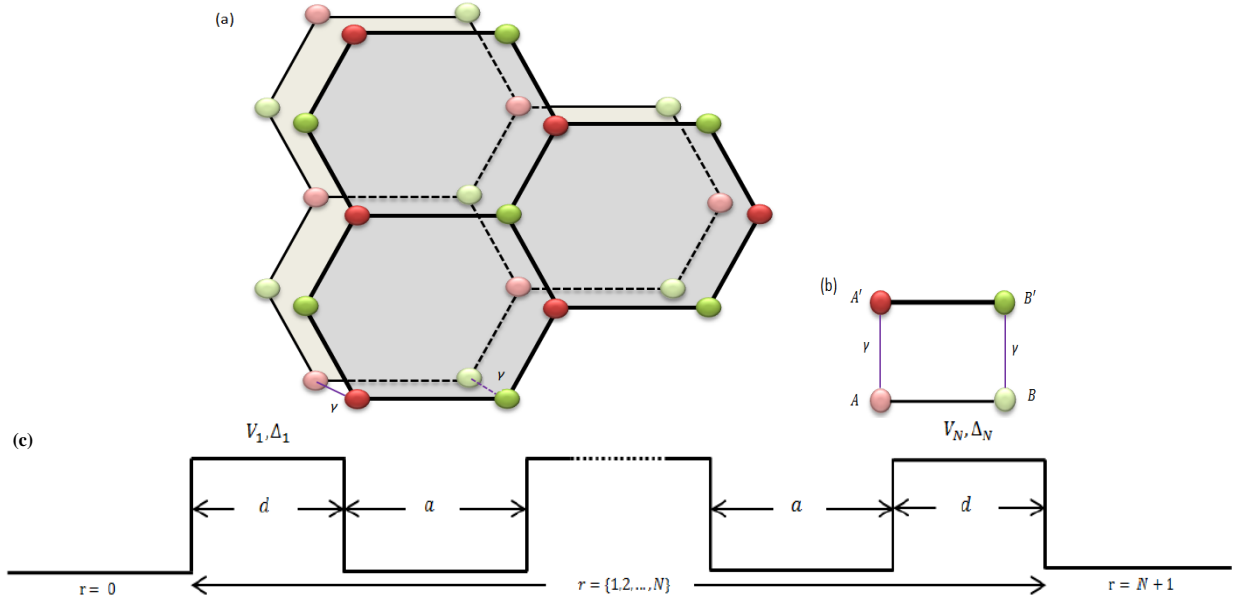


Figure 1: (a): Illustration of lattice structure of AA-stacked bilayer graphene, which is consisting of two coupled single layer graphene. (b): unit cell of AA-stacked consists of four atoms each pair is separated by an interlayer coupling energy of order $\gamma = 0.2 \text{ eV}$. (c): multibarrier structure consisting of $N + 2$ regions.

The charge carriers in the AA-stacked bilayer graphene are described, in each region r , by the following four-band Hamiltonian [23]

$$H_r = \begin{pmatrix} V_r + \Delta_r & v_F(p_x - ip_y) & \gamma & 0 \\ v_F(p_x + ip_y) & V_r - \Delta_r & 0 & \gamma \\ \gamma & 0 & V_r + \Delta_r & v_F(p_x - ip_y) \\ 0 & \gamma & v_F(p_x + ip_y) & V_r - \Delta_r \end{pmatrix}. \quad (1)$$

The eigenstates of H_r are the four component spinors $\Psi^r = (\Psi_A^r, \Psi_B^r, \Psi_{A'}^r, \Psi_{B'}^r)^T$, where $\Psi_{A(A')}$ and $\Psi_{B(B')}$ are the envelope functions associated with the probability amplitudes of the wave functions on the $A(A')$ and $B(B')$ sublattices of the lower (upper) layer. In (1), $p_{x,y} = -i\hbar\nabla_{x,y}$ is the in-plane momentum relative to the Dirac point, $v_F = 10^6 m/s$ is the Fermi velocity for electrons in single layer graphene, V_r is the potential heights and Δ_r is the gaps. In Figure 1(a), we have the bilayer graphene consisting of two layers of graphene having the structure AA-stacked, where the A sublattice of the top layer is stacked directly above the same sublattice of the bottom layer by the interlayer coupling $\gamma = 0.2 \text{ eV}$. The unit cell is consisting of four atoms labeled A, B on the lower layer and A', B' on the upper layer, see Figure 1(b).

We notice that our system is infinite along the y -direction since $[H_r, p_y] = 0$ and then we can decompose our spinor into

$$\Psi^r(x, y) = e^{ik_y y} \psi^r(x, k_y). \quad (2)$$

From the eigenvalue equation $H_r \Psi^r = E \Psi^r$, we end up with four linear differential equations of the form

$$-i\eta(\partial_x + k_y)\psi_B^r + \psi_{A'}^r = (E - V_r - \Delta_r)\psi_A^r \quad (3a)$$

$$-i\eta(\partial_x - k_y)\psi_A^r + \psi_{B'}^r = (E - V_r + \Delta_r)\psi_B^r \quad (3b)$$

$$-i\eta(\partial_x + k_y)\psi_{B'}^r + \psi_A^r = (E - V_r - \Delta_r)\psi_{A'}^r \quad (3c)$$

$$-i\eta(\partial_x - k_y)\psi_{A'}^r + \psi_B^r = (E - V_r + \Delta_r)\psi_{B'}^r \quad (3d)$$

where we have introduced the length scale $\eta = \frac{\hbar v_F}{\gamma} \approx 3.29 \text{ nm}$. From now on we switch to dimensionless quantities by measuring all energy terms in units of the interlayer coupling γ , namely $E \rightarrow \frac{E}{\gamma}$, $V_r \rightarrow \frac{V_r}{\gamma}$ and $\Delta_r \rightarrow \frac{\Delta_r}{\gamma}$. We combine the above equations to eliminate the unknown ones at time to end up with the following differential equation

$$[\partial_x^2 + (k_r^\tau)^2] \psi_B^r(x, k_y) = 0 \quad (4)$$

where the wave vector along the x -direction reads as

$$k_r^\tau = \sqrt{-k_y^2 + \eta^{-2} \left((E - V_r - \tau)^2 - \Delta_r^2 \right)} \quad (5)$$

and τ is the cone index, with $\tau = -1$ ($\tau = +1$) for the lower (upper) cone. Then we have V_{2n-+1} and Δ_{2n-+1} equal to V_1 and Δ_1 , respectively. For the regions where $V_1 = \Delta_1 = 0$, we find the wave vector

$$k_0^\tau = \sqrt{-k_y^2 + \eta^{-2} (E - \tau)^2} \quad (6)$$

and the corresponding energy band is

$$E^{s_0, \tau} = \tau + s_0 \sqrt{\eta^2 ((k_0^\tau)^2 + (k_y)^2)}. \quad (7)$$

However generally, for any region we can deduce the energy from previous analysis as

$$E^{s, \tau} = V_1 + \tau + s_1 \sqrt{\eta^2 ((k_1^\tau)^2 + (k_y)^2) + \Delta_1^2} \quad (8)$$

where s_1 is the chirality index of a quasiparticle in the barrier regions ($V_r = V_1$, $\Delta_r = \Delta_1$) and in outside ($V_r = \Delta_r = 0$) is s_0 , with $s_1 = +1$ (or $s_0 = +1$) and $s_1 = -1$ (or $s_0 = -1$) are the electron-like

and hole-like band indexes. It is important to note that in (8), for $\gamma \rightarrow 0$, the energy bands will be reduced to

$$E^s = V_1 + s_1 \sqrt{\hbar v_F((k_1^\tau)^2 + (k_y)^2) + \Delta_1^2} \quad (9)$$

which is a degenerate energy and corresponding to two monolayers. It is clear that this degeneracy can be lifted by taking into account the coupling between the two monolayers, i.e. $\gamma \neq 0$ [28].

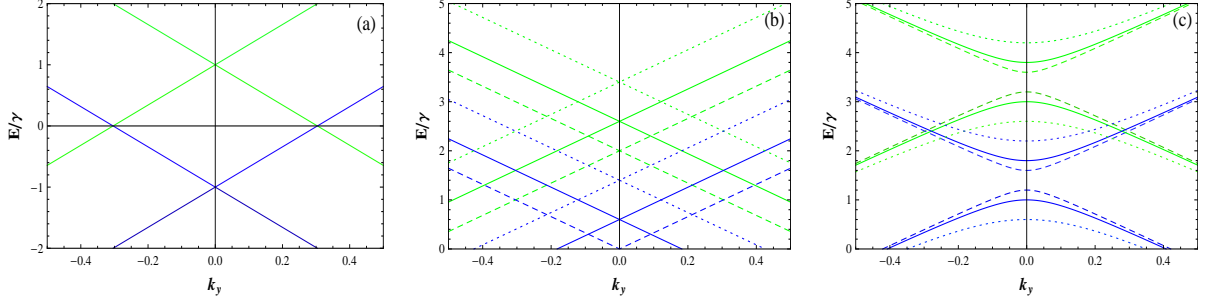


Figure 2: The energy bands as a function of the momentum k_y , where the blue line (green line) corresponds to the lower cone (upper cone). (a): for $V_1 = \Delta_1 = 0$. (b): for $\Delta_1 = 0$ and $V_1 = (\gamma, 1.6\gamma, 2.4\gamma)$ correspond to (dashed line, solid line, dotted line). (c): for $V_1 = 2.4\gamma$ and $\Delta_1 = (0.2\gamma, 0.4\gamma, 0.8\gamma)$ correspond to (dashed line, solid line, dotted line).

In Figure 2, we plot the energy bands as a function of the momentum k_y for the lower cone $\tau = -1$ (blue line) and the upper cone $\tau = 1$ (green line). In Figures 2(a) and 2(b) the energy bands are plotted for $\Delta_1 = 0$ while in Figure 2(c) for $\Delta_1 \neq 0$. It is evident that in Figure 2 the energy bands are just the double copies of monolayer graphene bands, with one Dirac point is shifted to wards positive ($\tau = +1$) and the other towards negative ($\tau = -1$) energies. For zero gap the spectrum is linear (Figures 2(a) and 2(b)), however for a finite gap the spectrum is parabolic (Figures 2(c)). In Figure 2(b), we plot the energy bands for three different values of the potential heights $V_1 = (\gamma, 1.6\gamma, 2.4\gamma)$. From this, we can observe that when we increase the potential heights V_1 , the energy bands increase upwards. To see the effect of the gap, we plot the energy bands for three different values of $\Delta_1 = (0.2\gamma, 0.4\gamma, 0.8\gamma)$ and for $V_1 = 2.4\gamma$, the results are shown in Figure 2(c). It is clearly seen that a gap appears at each of the two Dirac points ($V_1 + \tau - \Delta_1 < E < V_1 + \tau + \Delta_1$). When we increases Δ_1 , the width of these gaps increases as well.

Figure 3 represents the band structure of AA-stacked bilayer graphene for zero and finite gap. For $r = 0$, which corresponds to the incident region, the electron states can be subdivided into two regimes. The first one is where both $\tau = \pm 1$ electrons are electron-like, the second one is where $\tau = +1$ electrons are hole-like while $\tau = -1$ electrons are electron-like. However, for the transmission region ($r = N + 1$), we have two regimes as we shall show in the incident region. Note that we have four transmissions that are related to the band structures on the incident and transmission region. In addition, we notice that for the intracone transitions (i.e. $\tau \rightarrow \tau$ processes), there exist four cases for transitions across the barrier:

- Electron in regime I \rightarrow Electron in regime I (1)
- Electron in regime I \rightarrow Electron in regime II (2)

- Electron in regime II \rightarrow Electron in regime I (3)

- Electron in regime II \rightarrow Electron in regime II (4)

However, all intercone transitions (*i.e.* $\tau \rightarrow -\tau$ processes) are strictly forbidden due to the orthogonality of electron wave functions with a different cone index [24]. As already mentioned above, the transitions depend on the incident and transmission regions, so they depend anywhere in the presence or absence of the gap. For each of the four cases for transitions, the transmission can be calculated using the same method.

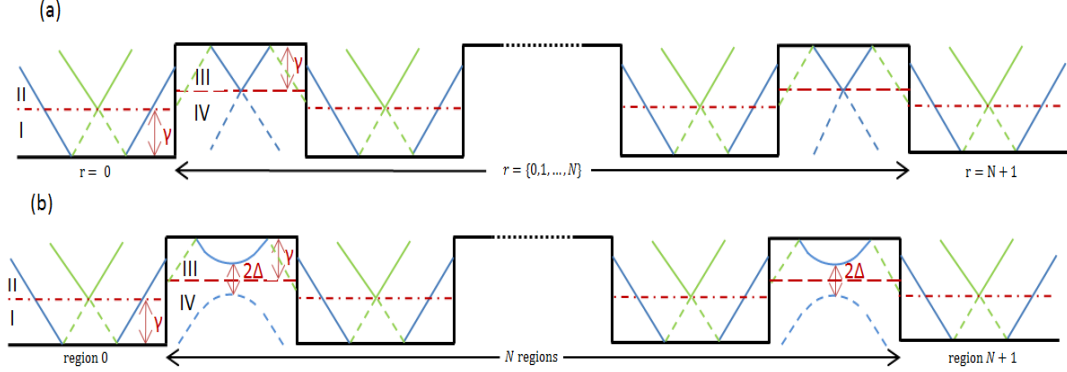


Figure 3: Schematic representation of the band structures. (a): for the barriers structure with zero gap. (b): for the barriers structure with finite gap.

3 Transmission probability

Next we shall show in detail the calculation of the transmission probability of electrons across the periodic barrier structure in our AA-stacked bilayer graphene system. The wave function solution of the system in each region r can then be written in terms of a matrix form as

$$\psi^r = G_r \cdot M_r \cdot A_r \quad (10)$$

where different matrices are given by

$$G_r = \begin{pmatrix} s_r \tau f_r^{\tau,+} & s_r \tau f_r^{\tau,-} \\ \tau & \tau \end{pmatrix}, \quad M_r = \begin{pmatrix} e^{ik_r^\tau x} & 0 \\ 0 & e^{-ik_r^\tau x} \end{pmatrix}, \quad A_r^\tau = \begin{pmatrix} \alpha_r^\tau \\ \beta_r^\tau \end{pmatrix} \quad (11)$$

such that $f_r^{\tau,\pm}$ reads as

$$f_r^{\tau,\pm} = \pm \sqrt{\frac{E - V_1 - \tau + \Delta_1}{E - V_1 - \tau - \Delta_1}} e^{\mp i \phi_r^\tau} \quad (12)$$

and the phase is defined by

$$\phi_r^\tau = \arctan(k_y/k_r^\tau). \quad (13)$$

We are interested in the normalization coefficients, namely the components of A_r^τ , on the both sides of the multibarrier structure. In other words, for the incident region ($r = 0$) and transmission region ($r = N + 1$), respectively, we have

$$A_0^\tau = (1, r^\tau)^T, \quad A_{N+1}^\tau = (t^\tau, 0)^T \quad (14)$$

where r^τ and t^τ are the reflection and transmission coefficients of each cone ($\tau = \pm 1$), respectively. We use two different matrix notation written as

$$G_{2n_+} \cdot M_{2n_+} = G_0 \cdot M_0, \quad G_{2n_-+1} \cdot M_{2n_-+1} = G_1 \cdot M_1 \quad (15)$$

where we have $V_1 = \Delta_1 = 0$ in $r = 2n_+$ and $V_1 \neq 0$ and $\Delta_1 \neq 0$ for $r = 2n_- + 1$, with $n_\pm = \{0, 1, \dots, \frac{N\pm 1}{2}\}$. Using the boundary conditions and the transfer matrix method, we can connect A_0^τ with A_{N+1}^τ through the matrix ζ

$$\zeta = \prod_{j=0}^n M_0^{-1} [j(d+a)] \cdot G_0^{-1} \cdot G_1 \cdot M_1 [j(d+a)] \cdot M_1^{-1} [(j+1)d+ja] \cdot G_1^{-1} \cdot G_0 \cdot M_0 [(j+1)d+ja]. \quad (16)$$

Consequently, we have two channels for the transmission probability in each individual cone, which are given by

$$T^\tau = \frac{1}{[\zeta_{11}]^2} \quad (17)$$

where ζ_{11} is a element of the matrix ζ .

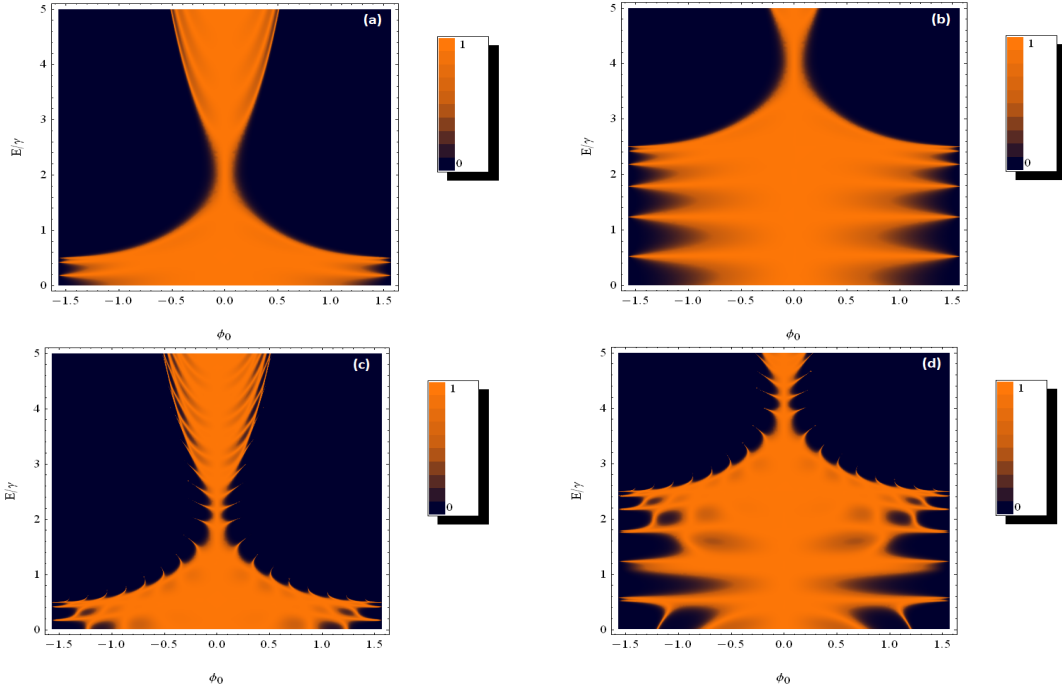


Figure 4: Density plot of transmission probability as a function of the incident angle ϕ_0 and its energy E , for $V_1 = 3\gamma$, $a = 2d = 30 \text{ nm}$ and $\Delta_1 = 0\gamma$. (a)/(b) for single barrier with $\tau = -1/\tau = 1$. (c)/(d) for double barrier with $\tau = -1/\tau = 1$.

To allow for a suitable interpretation of our main results, we compute numerically the transmission probabilities for $\tau = 1$ and $\tau = -1$. In what follow we start by studying the transmission probability for single, double barrier and finite periodic barrier structures. We first consider the case of single

and double barrier geometry with zero gap. In Figure 4 we show the density plot of the transmission probability as a function of the incident angle and its energy. The different colors from blue to orange correspond to different values of the transmission from 0 to 1. It is important to note that in the case of AA-stacked bilayer graphene the band structure is composed of two Dirac cones shifted by $\tau = -1$ (Figures 4(a) and 4(c)) and $\tau = 1$ (Figures 4(b) and 4(d)). In addition, the transmission probabilities, for $\tau = -1$ and $\tau = 1$, have the same form as that in the case of single layer graphene [14]. In both cases of single layer and AA-stacked bilayer graphene, around the point $\phi_0 = 0$, we have perfect transmission with a manifestation of the Klein tunneling effect [6]. Until now we notice that there is some similarity between single layer and AA-stacked bilayer graphene. However, for AA-stacked bilayer graphene both the electrons and holes have the same chirality index $s = \pm 1$ while in the case of single layer graphene the electron has always $+1$ and -1 for the hole. For the transmission of the lower layer (Figures 4(a) and 4(c)) the Dirac points correspond to $E = V_1 - 1$ and for the upper layer (Figures 4(b) and 4(d)) correspond to $E = V_1 + 1$. The results for a symmetrical double barrier structure of width d and interbarrier separation a , are shown in Figures 4(c) and 4(d). Compared to the results seen above for single barrier, we observe the appearance of peaks in transmission probability.

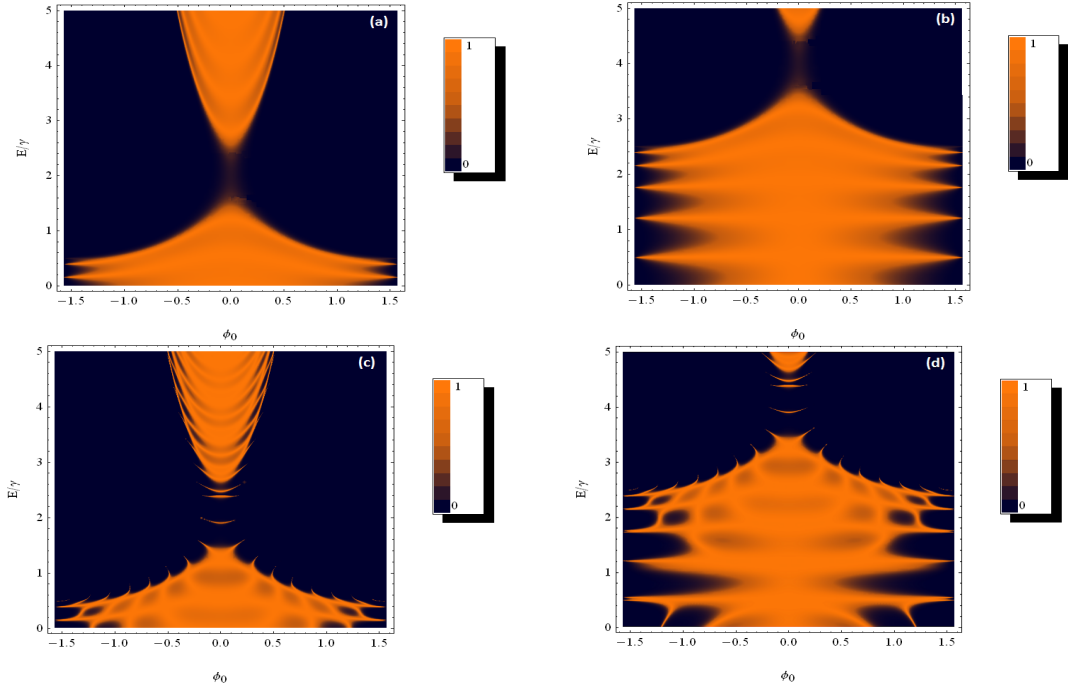


Figure 5: Density plot of transmission probability as a function of the incident angle ϕ_0 and its energy E , for $V_1 = 3\gamma$, $a = 2d = 30 \text{ nm}$ and $\Delta_1 = 0.4\gamma$. (a)/(b) for single barrier with $\tau = -1/\tau = 1$. (c)/(d) for double barrier with $\tau = -1/\tau = 1$.

Now let us see what will happen if we introduce a gap in the band structures. To do this, we extend the results presented in Figure 4 to the case $\Delta_1 = 0.4\gamma$ to get Figure 5. It is clearly shown that, in contrast to the single barrier case (Figures 5(a) and 5(b)), there are full transmission resonances, in the case of double barrier (Figures 5(c) and 5(d)), inside the gap ($V_1 + \tau - \Delta_1 < E < V_1 + \tau + \Delta_1$). Note that, the transmission resonances are resulting from the available states in the well between the

barriers. As already mentioned above, for a gapless graphene we have perfect transmission that is a manifestation of Klein tunneling effect. In addition, it may be noted that the opening gap in the barrier region suppresses this effect.

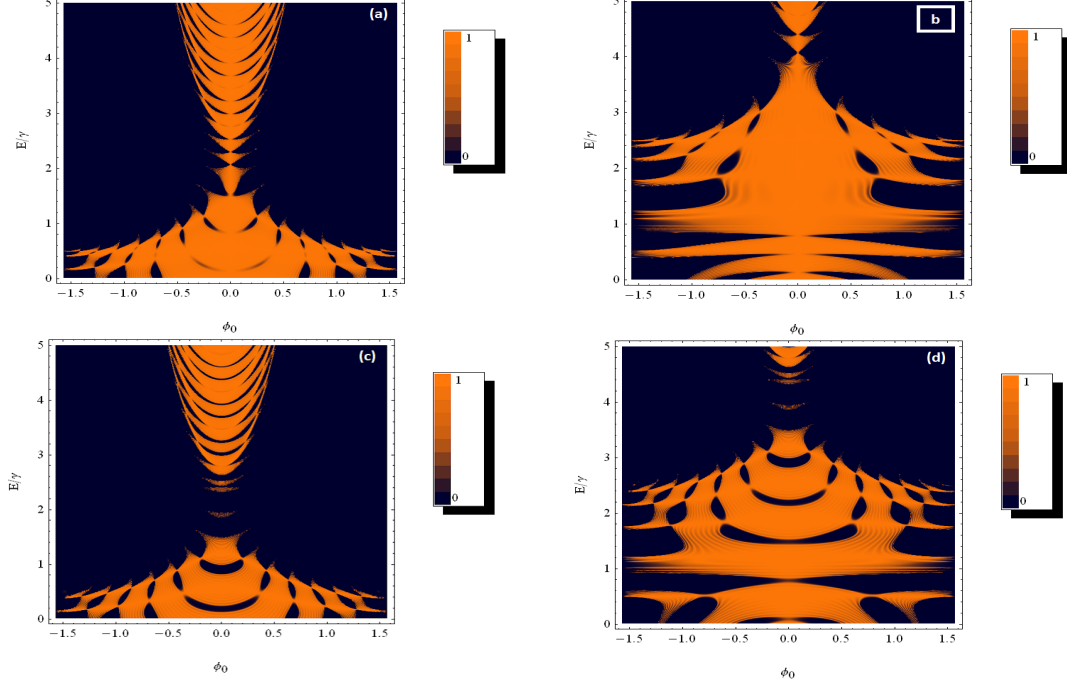


Figure 6: Density plot of transmission probability as a function of the incident angle ϕ_0 and its energy E , for finite periodic barrier structure that contain 25 regions, with $V_1 = 3$ and $a = 2d = 30 \text{ nm}$. (a)/(c) for $\tau = -1$ with $\Delta_1 = 0 / \Delta_1 = 0.4\gamma$. (b)/(d) for $\tau = 1$ with $\Delta_1 = 0 / \Delta_1 = 0.4\gamma$.

Next we consider the finite periodic barrier structure that contain 25 regions. In Figure 6 we show the transmission probabilities, associated with $\tau = \pm 1$, as a function of the incident angle ϕ_0 and its energy E , for $V_1 = 3$ and $a = 2d = 30 \text{ nm}$. Figures 6 (a)/(c) for $\Delta_1 = 0 / \Delta_1 = 0.4\gamma$ and $\tau = -1$ while Figures 6 (b)/(d) for $\Delta_1 = 0 / \Delta_1 = 0.4\gamma$ and $\tau = +1$. It is evident that the band structure of such barrier can have more than one Dirac points located at $E = V_1 - 1$ for the lower cone (Figure 6(a)) and at $E = V_1 + 1$ for the upper cone (Figure 6(b)). It is important to note that the location of Dirac point does not depend on the number of barriers. In fact, the position of the Dirac point is the same for single, double and the periodic barrier structures. However, increasing the number of barrier leads to the occurrence of resonance peaks in the transmission probability. These resonance peaks correspond to the positions of new cone index like associated with $\tau = \pm 1$ (Figures 6(a) and 6(b)) in the finite periodic barrier structures. We should emphasize that for $\tau \rightarrow 0$, our system will be reduced to the case of single layer graphene [14, 29]. From Figure 6(c) and 6(d), we can clearly see that the presence of the gap leads to suppression of the Klein tunneling effect [6]. In addition, it is important to note that the number of peaks presented inside the transmission gap ($V_1 + \tau - \Delta_1 < E < V_1 + \tau + \Delta_1$), in the case of double barrier structure (Figure 5(c) and 5(d)), is the same as that corresponding to the transmission trough finite periodic barrier structure.

4 Conductance

Basing on the obtained results above regarding the transmission probabilities of our system, we will see how the two conductance (G^τ) of each cone channel ($\tau = \pm 1$) will behave. For this purpose, we evaluate G^τ by using the Landauer-Büttiker [30] formula

$$G^\tau = G_0 \int_0^{\frac{\pi}{2}} T^\tau(E, \phi_0) \cos \phi_0 d\phi_0 \quad (18)$$

where the unit conductance

$$G_0 = NL_y k_F e^2 / h\pi \quad (19)$$

with the factor $N = 4$ is due to the spin and valley degeneracy, L_y is the width of the sample in the y -direction and

$$k_F = \sqrt{k_y^2 + (k_0^\tau)^2} = s_0 \eta^{-1} (E - \tau). \quad (20)$$

The total conductance G_t is defined as the sum of the conductance channels in each individual cone (G^τ) such as [24]

$$G_t = \frac{1}{2} (G^+ + G^-) \quad (21)$$

and the factor $1/2$ is required because the total conductance is contribution of the two cones. Whereas, in the case of AB-stacked bilayer graphene, there are four transmissions channels, then the total conductance is the sum of four conductances channels [27]. In the forthcoming analysis, we evaluate numerically the conductance in AA-stacked bilayer graphene.

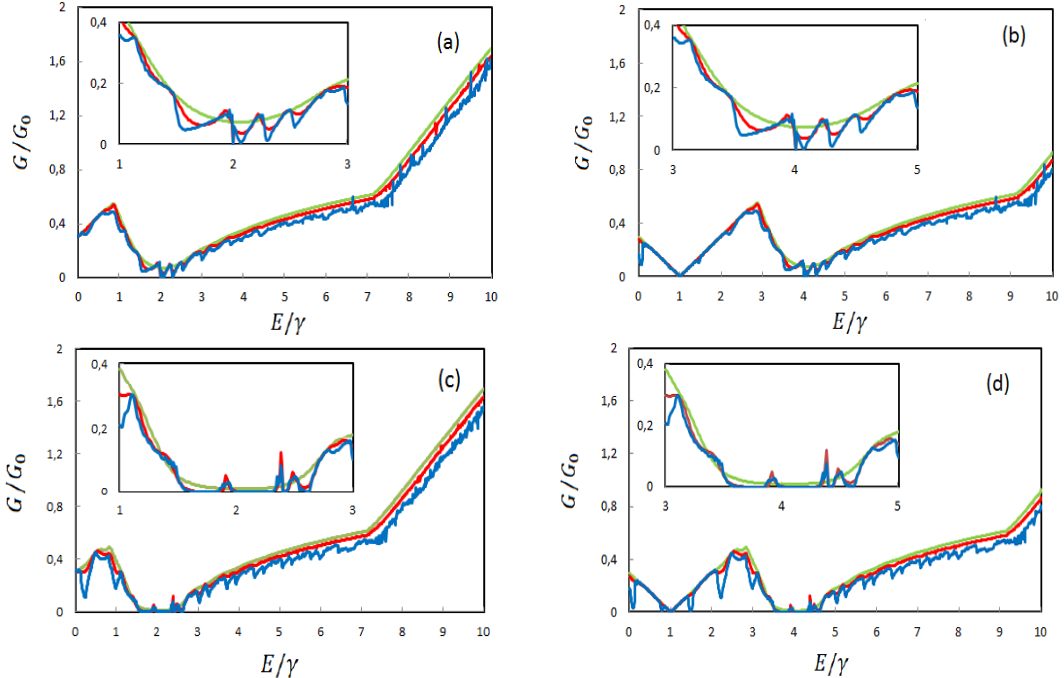


Figure 7: Conductance in each individual cone as a function of the energy for $a = 2d = 30 \text{ nm}$ and $V_1 = 3$, with single (green line) and double (red line) barrier structure and also periodic barrier contain 25 regions (blue line). (a)/(c) for $\tau = -1$ and $\Delta_1 = 0/\Delta_1 = 0.4\gamma$. (b)/(d) for $\tau = 1$ and $\Delta_1 = 0/\Delta_1 = 0.4\gamma$

We present in Figure 7 the conductance in each individual cone, given in (18), for a single (green line), double barriers (red line) and also for a finite periodic barrier contain 25 regions (blue line), as a function of the energy E , for $V_1 = 3$ and $a = 2d = 30 \text{ nm}$. In Figures 7(a) and 7(b) the conductances are plotted for $\Delta_1 = 0$ while in Figure 7(c) and 7(d) for $\Delta_1 = 0.4$. It is important to note that, in the case of single, double and finite periodic barriers, we have the same position of the Dirac point for each individual cone ($E = V_1 - 1$ in Figure 7(a) and $E = V_1 + 1$ in Figure 7(b)). We conclude that the position of the Dirac point is the same whatever the number of the barriers. In addition, for the case of finite periodic barrier we can have more than one Dirac point at the same position. Moreover, when we increase the number of barrier the conductance decrease and new peaks appear. To see how the gap will affect the conductance channel in each cone ($\tau = \pm 1$), we extend the results presented in Figures 7(a) and 7(b) to the case $\Delta_1 = 0.4\gamma$ to get Figures 7(c) and 7(d). For the case of single barrier (green line), the conductance is zero and there are no resonances in the regime of energy ($V_1 + \tau - \Delta_1 < E < V_1 + \tau + \Delta_1$). However, for the double barrier structure (red line) new peaks of resonances appear in the above mentioned regime of energy. These peaks can be attributed to the bound electron states in the well region between the barriers. The number of these peaks, in the regime of energy ($V_1 + \tau - \Delta_1 < E < V_1 + \tau + \Delta_1$), is the same as that of the finite periodic barrier.

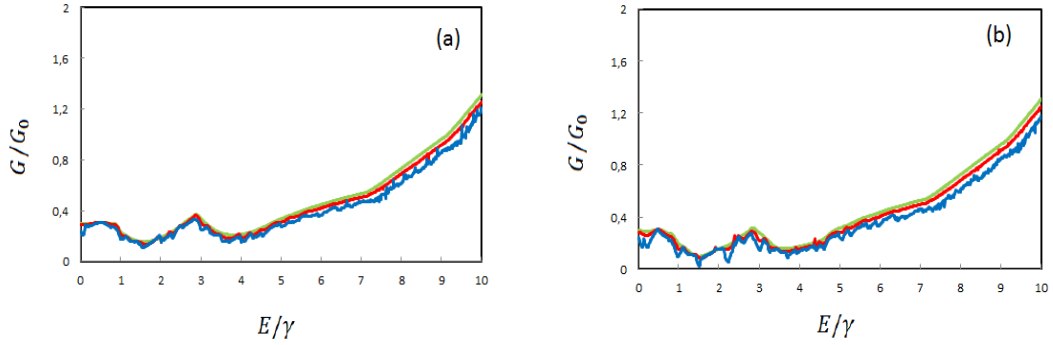


Figure 8: Total conductance as a function of energy, for $V_1 = 3$ and $a = 2d = 30 \text{ nm}$, with single (green line) and double (red line) barrier structure and also finite periodic barrier contain 25 regions (blue line). (a) for $\Delta_1 = 0$ and (b) for $\Delta_1 = 0.4\gamma$

Now, we plot the total conductance (21) as a function of energy for single (green line), double (red line) barrier structure and for finite periodic barrier contain 25 regions (blue line). Indeed, the existence of the intracone transition allows only two transmission channels in AA-stacked bilayer graphene [24] resulting in a total conductance, while the transmission in the intercone is zero. In contrast, for AB-stacked bilayer graphene [27] we have intracone and intercone transitions, which are possible between all four bands. In addition, the total conductance of AA-stacked bilayer graphene is different with that of the single layer graphene [14].

5 Conclusion

We have studied the electronic transport of electrons through single, double and finite periodic barrier on the AA-stacked bilayer graphene. as well as analyzed the transmission probability and corresponding conductance we have started by formulating our Hamiltonian model that describes the system under consideration and getting the associated energy bands. The obtained bands are composed of two Dirac cones shifted up and down by the interlayer coupling.

Subsequently, we have calculated the transmission probabilities and presented numerically the results for each individual cone ($\tau = \pm 1$). For AA-stacked bilayer graphene the transmission in the intercone is zero, in contrast, for AB-stacked bilayer graphene where we have intracone and intercone transitions. By increasing the number of barriers an occurrence of resonance peaks in the transmission probabilities. These resonance peaks correspond to the positions of new cones index like associated with $\tau = \pm 1$ in the finite periodic barrier structures. However, the location of Dirac point ($E = V_1 + \tau$) does not depend on the number of barriers. For a gapless graphene we have perfect transmission that is a manifestation of Klein tunneling. However, the opening gap in the barrier region leads to suppression of the Klein tunneling effect for near-normal incidence.

Basing on the obtained results for the transmission probabilities we have found that there are two conductance channels through different barriers cases. In the case of finite periodic barrier we can have more than one Dirac point at the same position. Also, we have investigated the effect of the gap on the conductance channel in each cone. It was noticed that in the well region between the barriers the appearance of new peaks of resonances, which can be attributed to the bound electron states. Finally the total conductance studied as an average of the two conductance channels in each cone and we have concluded that this later for AA-stacked bilayer graphene is different with that corresponding to single layer graphene.

Acknowledgment

The generous support provided by the Saudi Center for Theoretical Physics (SCTP) is highly appreciated by all authors.

References

- [1] K. S. Novosolov, A. K. Geim, S. V. Morozov, D. Jiang, Y. Zhang, S. V. Dubonos, I. V. Gregorieva, and A. A. Firsov, *Science* 306, 666 (2004).
- [2] A. H. Castro Neto, F. Guinea, N. M. R. Peres, K. S. Novoselov, and A. K. Geim, *Reviews of Modern Physics* 81, 109 (2009).
- [3] N. M. R. Peres, *Reviews of Modern Physics* 82, 2673 (2010).
- [4] D. S. L. Abergel, V. Apalkov, J. Berashevich, K. Ziegler, and T. Chakraborty, *Advanced Physics* 59, 261 (2010).
- [5] T. Ando, *Physica E* 40, 213 (2007).

- [6] M. I. Katsnelson, K. S. Novoselov, and A. K. Geim, *Nature Physics* 2, 9 (2006).
- [7] J. D. Bernal, *Physical and Engineering Sciences* 106, 749 (1924).
- [8] J.-K. Lee, S.-C. Lee, J.-P. Ahn, S.-C. Kim, J. I. B. Wilson, and P. John, *Journal of Chemical Physics* 129, 234709 (2008).
- [9] P.L. de Andres, R. Ramirez, and J. A. Vergés, *Physical Review B* 77, 045403 (2008).
- [10] Z. Liu, K. Suenaga, P. J. F. Harris, and S. Iijima, *Physical Review Letters* 102, 015501 (2009).
- [11] Y.-H. Ho, J.-Y. Wu, R.-B. Chen, Y.-H. Chiu, and M.-F. Lin, *Applied Physics Letters* 97, 101905 (2010).
- [12] J. Borysiuk, J. Soltys, and J. Piechota, *Journal of Applied Physics* 109, 093523 (2011).
- [13] I. Lobato, and B. Partoens, *Physical Review B* 83, 165429 (2011).
- [14] E. S. Azarova, and G. M. Maksimova, *Physica E* 61, 118 (2014).
- [15] C.-H. Park, L. Yang, Y.-W. Son, M. L. Cohen, and S. G. Louie, *Nature Physics* 4, 213 (2008).
- [16] S. Ghosh, and M. Sharma, *Journal of Physics: Condensed Matter* 21, 292204 (2009).
- [17] Y. P. Bliokh, V. Freilikher, S. Savel'ev, and F. Nori, *Physical Review B* 79, 075123 (2009).
- [18] I. Snyman, *Physical Review B* 80, 054303 (2009).
- [19] R. Nasir, K. Sabeeh, and M. Tahir, *Physical Review B* 81, 085402 (2010).
- [20] M. Barbier, F. M. Peeters, P. Vasilopoulos, and J. M. Pereira, Jr., *Physical Review B* 77, 115446 (2008).
- [21] C. Bai, and X. Zhang, *Physical Review B* 76, 075430 (2007).
- [22] M. Barbier, P. Vasilopoulos, F. M. Peeters, and J. M. Pereira, Jr., *Phys. Rev. B* 79, 155402 (2009).
- [23] C. J. Tabert, and E. J. Nicol, *Physical Review B* 86, 075439 (2012).
- [24] M. Sanderson, Y. S. Ang, and C. Zhang, *Physical Review B* 88, 245404 (2013).
- [25] C. Bena, and G. Montambaux, *New Journal of Physics* 11, 095003 (2009).
- [26] A. L. Rakhmanov, A. V. Rozhkov, A. O. Sboychakov, and F. Nori, *Physical Review Letters* 109, 206801 (2012).
- [27] B. V. Duppen, and F. M. Peeters, *Physical Review B* 87, 205427 (2013).
- [28] A. Dyrdał, and J. Barnaś, *Solid State Communications* 188, 27 (2014).
- [29] G. M. Maksimova, E. S. Azarova, A. V. Telezhnikov, and V. A. Burdov, *Physical Review B* 86, 295422 (2012).
- [30] Ya. M. Blanter, and M. Büttiker, *Physics Reports* 336, 1 (2000).